

# Optical Actuation of a Bistable MEMS

Marc Sulfridge, Taher Saif, Norman Miller, and Keith O'Hara

**Abstract**—This paper presents an optical actuation scheme for MEMS devices based on the well-established fact that light possesses momentum, and hence, imparts a force equal to  $2W/c$  when reflected by a surface. Here,  $W$  is the total power of the reflected light, and  $c$  is the speed of light. Radiation pressure, as it is known, is nearly insignificant for most macroscale applications, but it can be quite significant for MEMS devices. In addition, light actuation offers a new paradigm. First, intersecting light beams do not interfere, in contrast to electrical conductors, which short when they come into contact. Second, light can operate in high temperature and high radiation environments far outside the capability of solid state electronic components [10]. This actuation method is demonstrated, both in air and in vacuum, by switching the state of a bistable MEMS device. The associated heat transfer model is also presented. [771]

## I. INTRODUCTION

LIGHT has been used to manipulate MEMS devices for a number of years using a variety of different mechanisms. The earliest literature found on the subject used beams of light to heat various structures or membranes [8], [37], [14], [13], [9], [15], [3], [21], [19], causing thermal actuation.

Recently, a variation on this technique was presented in [17], [16]. The movement of a single crystal silicon disk in close proximity to a substrate creates optical interference (constructive or destructive depending on distance) which modifies the amount of absorption in the disk along its perimeter. The resulting nonuniform heating deforms the disk, giving rise to a parametric excitation, which in turn causes the disk to resonate.

Well into the 1990s, this optothermal actuation scheme was the only optical actuation mechanism found in the literature. In 1996, a new actuation mechanism was presented which employed optical, electrical, and mechanical energy [12]. Light is used to generate electron-hole pairs in a p-n junction. The charge separation creates an electric field which pulls down a mechanical beam that is in ohmic contact with the junction and is located above it. This movement, in turn, interferes with the optical path, thus creating a resonator.

Thakoor [20] exposed a polarized ceramic wafer to illumination close to the bandgap energy of the ceramic, which generates a large photovoltage. The piezoceramic deflects due to the inverse piezoelectric effect.

Datskos [18] and Roan [10] used photo-induced stress to bend small cantilevers. Such stress is created when a crystalline lattice absorbs a photon, thus promoting an electron from the valence to the conduction band. Essentially, this leaves a hole in the lattice close to the surface, causing it to contract slightly. Surface strain develops which deforms the beam.

To the authors' knowledge, Koehler [25] was the first to propose electromagnetic momentum (also known as radiation pressure) as the mechanism for actuating MEMS devices. However, this was a purely theoretical paper. Experimental validation of this mechanism was demonstrated in [5] by deflecting the tip of a cantilever. The very small deflections were detected by measuring the tunneling current between the cantilever tip and the substrate. In 2000, the mechanism was once again verified [11] on nanometer scale thick silicon cantilevers. The emphasis in this paper was also on low power (and hence low force) deflections.

In the present paper, we present an experiment in which radiation pressure is used to switch the state of a micron thick bistable MEMS beam, causing it to toggle by up to 23 microns. The bistable system was studied earlier in [31], where the switching of state was caused by electrostatic force. A thermal analysis is conducted to estimate the temperature rise in the beam due to incident radiation. It is shown that several competing force generating mechanisms that may arise due to incident radiation are much smaller than that due to radiation pressure.

## II. LIGHT ACTUATION

The ability to use light as an actuation mechanism is based on the fact that light possesses momentum. Hence, when it is absorbed by, or reflected off of a body, it exerts a pressure (radiation pressure) on that body, a fact first predicted by Maxwell [26], and later derived from both the particle and wave classical theories [4] as well as from quantum mechanical theory [22]. Radiation pressure was first experimentally verified in the famous Nichols-Hull experiment [28], in spite of the fact that the effect is very small under ordinary, macroscale conditions. Under some extreme conditions it is very influential even at the macroscale. For example, radiation pressure helps to counteract the crushing gravitational force at the cores of supermassive stars [32]. In addition, it is the dominant disturbance mechanism for the attitude control of satellites and space probes with asymmetric cross sections. It creates a torque about the center of mass of such a satellite (due to the asymmetry of the cross-sectional area), causing it to rotate [30].

### A. Radiation Pressure Force Law

The momentum,  $\vec{p}$  of a photon of light is given by  $\vec{p} = \hbar \vec{k}$ , where  $\hbar$  is Dirac's constant (Planck's constant,  $h$ , divided by

Manuscript received October 24, 2001; revised February 15, 2002. This work was supported by NSF Grant ECS 0083155. The work of K. O'Hara was supported by the U.S. Department of Energy, Division of Materials Science, under Grant DEFG 02-91ER45439. Subject Editor T. Kenny.

M. Sulfridge, T. Saif, and N. Miller are with the Department of Mechanical and Industrial Engineering, University of Illinois at Urbana-Champaign, IL 61801 USA (e-mail: sulfridge@uiuc.edu; saif@uiuc.edu; nr-millr@uiuc.edu).

K. O'Hara is with the Frederick Seitz Materials Research Laboratory, University of Illinois at Urbana-Champaign, IL 61801 USA (e-mail: kohara@micromachines.com).

Digital Object Identifier 10.1109/JMEMS.2002.803417.

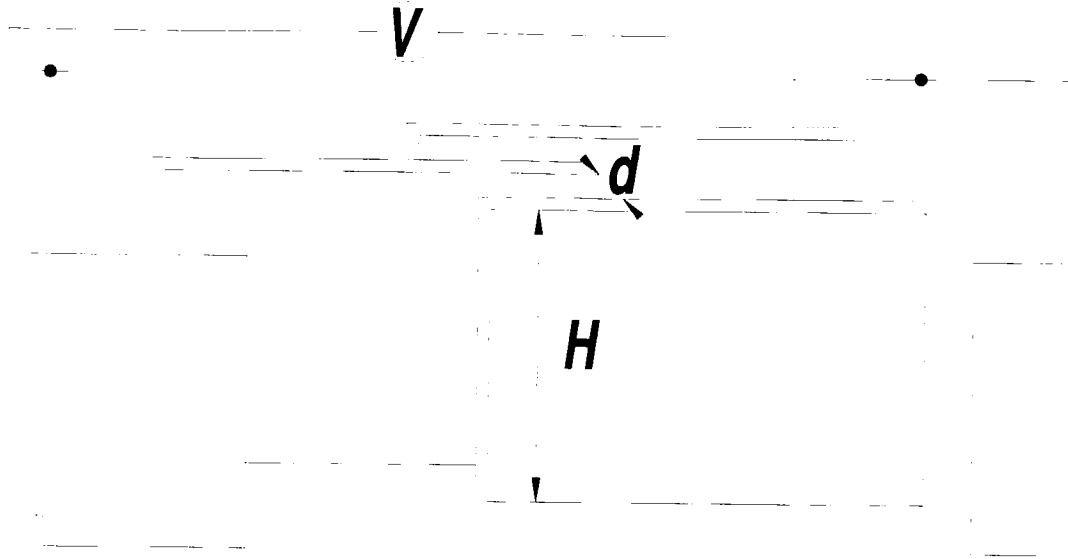


Fig. 1. Illustration of an electrostatic comb drive actuator.

$2\pi$ ), and  $\vec{k}$  is the vector wave number of the photon. The wave number is oriented in the direction of travel of the photon. It has a magnitude of  $2\pi/\lambda = \omega/c$  where  $\lambda$ ,  $\omega$ , and  $c$  are the wavelength, angular frequency, and speed of light, respectively. Thus,  $p = \hbar\omega/c = \hbar\nu/c$ , and we know that the energy,  $E$ , of the photon is given by  $E = h\nu$ . Hence,  $p = E/c$ .

If a large number of photons (all traveling in the same direction) are absorbed (i.e., stopped) by a body, then from Newton's second law, the force imparted on the body is given by  $F = dp/dt = (dE/dt)/c = W/c$ , where  $W$  is the power of the absorbed light. If, instead, the light is reflected by the body (i.e., its momentum is reversed), the force is doubled,  $F = 2W/c$ . Finally,  $W = IA$  where  $I$  is the average intensity of the light and  $A$  is the irradiated area. Thus, the forcing law is given by

$$F = 2 \frac{IA}{c}. \quad (1)$$

### B. Scaling

The obvious way to consider how the optical force,  $F$ , scales with the scale length,  $\ell$ , of the device is to assume that the light intensity is constant, which provides a rather attractive  $\ell^2$  scaling law. However, it is possible to focus the light as we scale the device, so that the intensity scales as  $\ell^{-2}$ , in which case  $F$  scales as  $\ell^0$ . Scaling in such a manner, however, has two important limitations. First, increasing the light intensity in this manner could lead to severe heating and possible device melting if any appreciable absorption takes place. In addition, light cannot be focused to a spot any smaller than its diffraction limit, which is on the order of the wavelength of the light.

Thus,  $F$  may scale as  $\ell^0$  down to some limit, at which point the scaling reverts to  $\ell^2$ . In either case, however, the scaling law is quite attractive. Similar scaling analysis of other actuation mechanisms [36] shows that electrostatic actuation also scales as  $\ell^2$ , while magnetic actuation scales somewhere between  $\ell^{2.5}$  and  $\ell^4$ . Note that force by thermal and piezoelectric actuation scales as  $\ell^2$  [24].

In order to get an estimate of optical force at MEMS scale, consider a 750 mW, normally incident laser beam focused to a

diameter of 10 microns perfectly reflected by a surface. Then the force on the surface  $F = 5$  nN [Equation (1)]. Now consider the force produced by the single electrostatic comb actuator shown in Fig. 1. The force law for such actuators is  $F = \epsilon_0 \epsilon_r h V^2 / d$ . For typical values of  $h = 10$   $\mu\text{m}$ ,  $d = 2$   $\mu\text{m}$ , and  $V = 10$  V,  $F = 4.43$  nN, comparable to optical force. Thus, we may conclude that radiation pressure is a potentially viable actuating mechanism for some MEMS devices.

### C. Benefits and Limitations

In addition to favorable scaling, optical actuation works equally well at elevated temperatures and in high radiation environments [10], provided that the light source is external to the harsh environment. This is possible to achieve by using lasers or fiber optics. In fact, in the experiment we present, the laser was located more than a meter from the device under test. More importantly, beams of light can cross without interfering with each other, making complex interconnectivity in a two dimensional environment possible. And using lasers, the power source for light actuated devices can be located far from the devices themselves. However, radiation pressure is subject to a number of limitations, as well.

1) *The Diffraction Limit:* The diffraction limit sets the minimum spot size of the light to  $D_{\min} = 2\lambda f / \pi D_0$  [33], where  $f$  is the focal length of the lens,  $\lambda$  is the wavelength of the light, and  $D_0$  is the laser diameter (defined as the  $2\sigma$  full width of the Gaussian beam intensity). If it is necessary to reduce the scale of a device beyond the diffraction limit of the light used, then at that point the scaling law becomes  $F \propto \ell^2$ , since the spot size of the light may be reduced no further.

2) *Laser Collimation:* A laser beam profile is not perfectly parallel, and in the far field it obeys the same inverse square intensity drop off from which all point sources suffer. However, within a distance known as the Rayleigh range, a laser beam remains nearly parallel. The actual beam profile is given by

$$D(z) = D_0 \sqrt{1 + \left( \frac{4\lambda z}{\pi D_0^2} \right)^2} \quad (2)$$

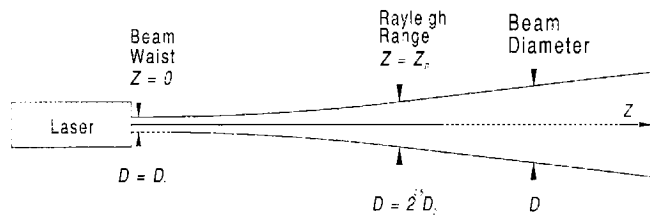


Fig. 2. Illustration of laser beam divergence. Note that the beam waist will actually be at the half silvered mirror of the laser's resonator cavity.

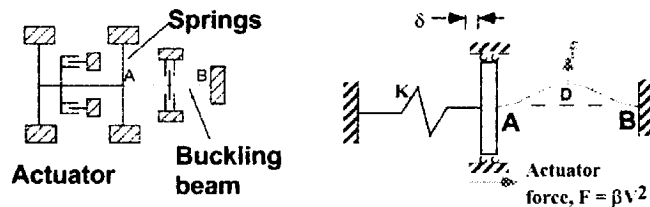


Fig. 3. Schematic and model of the bistable MEMS device used to test actuation by light.

and the Rayleigh range,  $z_R = \pi D_0^2 / 8\lambda$ , is defined as the distance at which the beam diameter grows to  $D_0\sqrt{2}$  (see Fig. 2). Note that for  $z > z_R$ , the laser cross section begins to limit to the cone  $D = 4\lambda z / \pi D_0^2$  [33], and consequently starts to obey the inverse square law.

For a typical red diode laser with an initial diameter of 5 mm, the Rayleigh range is a comfortable 15 m, which is why we generally think of laser beams as parallel. However, when the beam diameter is reduced to 50  $\mu\text{m}$ , the Rayleigh range shrinks to only 1.5 mm. Thus, if the travel distance of a laser beam is large within a MEMS device, it may require *in situ* recollimation.

3) *Absorption and Heating*: Radiation pressure is maximized for 100% reflective surfaces. No surface, however, is 100% reflective. If part of the power is simply transmitted through the device, there is no heating, but if the power is absorbed, the device will overheat. Thus it is essential to choose a combination of light wavelength and device material (or surface coating) for which the reflectivity is as high as possible, and the absorptivity is as low as possible. This issue will be covered in more detail later in the paper.

In Fig. 3, actuation by light is tested on a bistable MEMS device.

### III. A BISTABLE MEMS

The bistable MEMS device [31] shown in Fig. 4, consists of two long slender structural beams, made of single crystal silicon, and a comb drive actuator, *C*, that applies an axial compressive force on the beams to buckle them to a transverse displacement *D*. There are two possible buckled states and hence the system is bi-stable. Each beam is 1000  $\mu\text{m}$  long, 1  $\mu\text{m}$  wide and 15  $\mu\text{m}$  deep. They are attached in the middle so that they both buckle along the same direction with stability against rotation. The two beams can thus be considered as one beam AB. There is a small 3-comb actuator at the middle which may be employed to generate a threshold transverse force,  $f_{th}$ , on AB to switch its state, but  $f_{th}$  can also be generated by the radiation pressure of a laser focused on the lateral surface of the silicon beam.

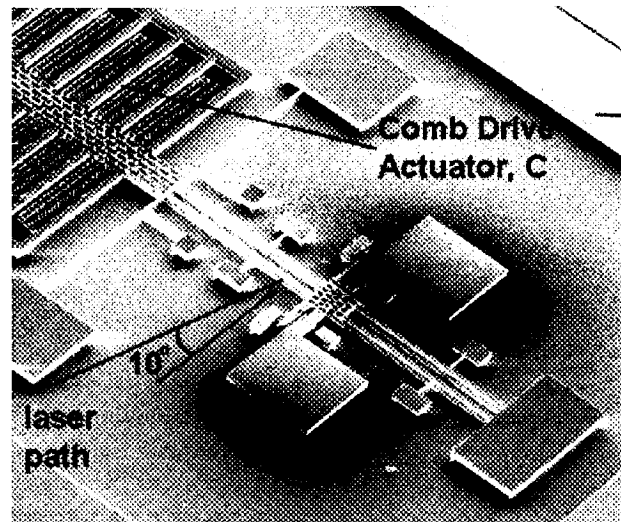


Fig. 4. SEM image of the bistable MEMS device.

#### A. Device Description

The reasons that this device was chosen are numerous. First, the force,  $f_{th}$  required to toggle the beam's buckled state is very small (only about 50 pN for a buckled displacement, *D*, of 3  $\mu\text{m}$ ), and hence it should be achievable by a single laser beam of moderate power (only about 10 mW when *D* is 3  $\mu\text{m}$ ). Second, using a bistable device makes it easy to determine how much force is generated, since it will remain in its initial state if the force is below the toggle threshold, and it will change states if the force is above that threshold. This eliminates any need to maintain the forcing mechanism for a long period of time. Additionally, the displacement of the toggle is very large compared to the force required, making the displacement relatively easy to accurately measure.

The device is also tunable (i.e., the beam, AB, can be buckled to any desired amount, *D*). Thus, a full data set of toggle threshold power versus buckled displacement can be generated, in order to confirm the mechanism of the actuation. Saif [31] showed that the toggle force,  $f_{th}$ , and hence the laser power, should be proportional to the cube of the buckled displacement. The threshold laser power quickly grows with increased buckle, and device heating considerations become very important. Since a wide range of displacement is needed for a complete data set, the device will have to hold up to relatively high power flux. For this reason, a thermal model is needed in order to establish a safe laser power range.

### IV. THERMAL MODEL

In order to estimate the temperature rise due to the absorption of light in silicon, a thermal model [see (3)] has been developed. It is a one dimensional model in which the entire beam loses heat through conduction through the beam, and convection and radiation through the ambient medium. In addition, the center of the beam absorbs heat within the footprint of the incident laser beam. Since laser beam cross-section is circular with a diameter equal to the height of the beam, and the model is one dimensional, the laser footprint is approximated by a rectangle with an area equal to the true footprint of the laser, and

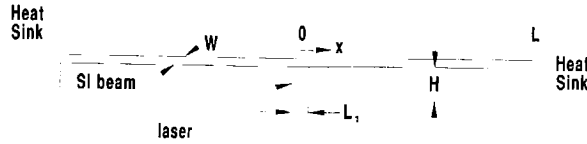


Fig. 5. Thermal model of the silicon beam.

a height equal to that of the beam. Hence, the half width of the rectangular footprint approximation is  $L_1 = 0.125\pi H$  where  $H$  is the height of the beam. The boundary conditions are no heat conduction across the centerline (symmetry) and constant temperature at the end of the beam (due to the large heat sink capacity of the substrate). The beam is initially considered to be at room temperature, although any initial condition can be set in the model.

The governing equation for the beam in terms of its temperature,  $T(x, t)$  is given by

$$\frac{\partial T}{\partial t} = \frac{1}{\rho c_p} \left( k_{si} \frac{\partial^2 T}{\partial x^2} + \frac{\partial k_{si}}{\partial x} \frac{\partial T}{\partial x} \right) + \frac{\alpha \dot{q}_l}{2L_1WH\rho c_p} - \frac{2(W+H)\epsilon\sigma}{WH\rho c_p} (T^4 - T_\infty^4) - \frac{2(W+H)h}{HW\rho c_p} (T - T_\infty)$$

$$\text{BCs} \quad \left. \frac{\partial T}{\partial x} \right|_{x=0} = 0 \quad T|_{x=L} = T_i$$

$$\text{IC} \quad T|_{t=0} = T_i.$$
(3)

All geometric parameters of (3) are identified in Fig. 5. Here,  $\dot{q}_l$  is the power of the laser beam,  $\sigma$  is the Stefan-Boltzmann constant,  $T_\infty$  is the temperature of the ambient air and surroundings,  $h$  is the free convection coefficient between the silicon beam and air for this geometry, and  $\epsilon$ ,  $k_{si}$ ,  $\alpha$ ,  $\rho$  and  $c_p$  are the emissivity, thermal conductivity, absorptivity, density and heat capacity, respectively, of silicon. The first term on the right hand side of the equation accounts for the conduction through the beam, the second term represents the absorbed laser power, the third term is the radiation of heat to the surroundings, and the last term is the free convection of heat to the ambient medium. In order to make use of this model, all of these parameters need to be determined as accurately as possible. We begin this determination by examining the optical properties of silicon.

#### A. Optical Properties

The optical properties that are needed in this model are reflectivity and absorption. Reflection is primarily a surface phenomenon which occurs whenever light passes through the interface between media of differing refractive indices. It is also greatly influenced by the phenomenon of thin film interference. Absorption is a volumetric phenomenon, which grows exponentially as a function of the depth through which the light passes. The mechanisms behind thin film interference and absorption will now be discussed in more detail.

1) *Thin Film Interference:* The thickness of the silicon beam used in this experiment is of similar order to the wavelength of light. Hence, it is necessary to consider the effects of thin film interference. This effect occurs because the light partially reflects off of both the front and the back faces of the silicon beam numerous times, creating multiple laser beams. When these beams

are in phase the beams reinforce each other, and when they are  $180^\circ$  out of phase they cancel [1]. Hence, for a beam of fixed thickness, reflection is a periodic function of the frequency of light reflected, having peaks corresponding to constructive interference, and troughs corresponding to destructive interference. Since all of the light that is not transmitted must be either reflected or absorbed, absorption exhibits similar periodicity.

2) *Absorption:* All primary absorption mechanisms involve the interaction of light with electrons [7], [27], [34], and hence the conductivity of a material has a great deal of influence on its absorptivity. In fact, Maxwell's equations in one dimension for linearly polarized light [2] simplify to

$$\frac{\partial^2 E}{\partial x^2} = \mu\epsilon \frac{\partial^2 E}{\partial t^2} + \mu\sigma_c \frac{\partial E}{\partial t} \quad (4)$$

where  $E$  is the electric field (transverse to the  $x$  direction),  $\mu$  is the magnetic permeability,  $\epsilon$  is the electric permittivity, and  $\sigma_c$  is the electrical conductivity. Obviously, this is the equation for a damped harmonic oscillator, and the amount of damping (i.e., absorption) is determined by the product of electrical conductivity and magnetic permeability. Hence, conductivity plays a strong role in determining absorption.

In practice, the solution to this equation is written in terms of the complex index of refraction,  $\tilde{n}$ , of the medium. The real part is referred to as the index of refraction,  $n$ , and is simply the ratio of the speed of light in vacuum to the speed of light in that medium. The imaginary part,  $k$ , is referred to as the absorption index, and it is the ratio of the wavelength of the light to its absorption depth (the depth at which the field drops to  $1/e$ ). Taken together,  $n$  and  $k$  are called the *optical constants* of the medium, and they are both functions of wavelength. The solution to Equation (4) in terms of these optical constants is given by

$$E = E_0 \text{Re} \left\{ \exp \left[ i\omega \left( -\frac{nx}{c_0} + t \right) \right] \exp \left[ -\frac{\omega kx}{c_0} \right] \right\} \quad (5)$$

where  $E_0$  is the initial field strength,  $c_0$  is the speed of light in vacuum, and  $\omega$  is the angular frequency of the light.

Values of the optical constants of silicon over a wide range of wavelength can be found in [6]. For the case of our thin silicon beam, the simple solution of Equation (5) must be modified to take into account thin film interference effects. This has been done using the algorithm presented in [2], and the results for absorption and reflectivity are shown in Figs. 6 and 7. These results are for intrinsic (i.e., undoped) silicon. Because it is readily available and has relatively high reflection (72%) with very low absorption ( $<1\%$ ) in our silicon beam, a 1064 nm Nd:YAG laser was chosen for this experiment, despite the fact that it is slightly above the band gap of silicon. In practice, the results obtained in the experiment to be described later in this paper best fit an absorption of about 2%, which is slightly higher than what we would expect from Fig. 6, and so an absorption of 2% is used in the thermal model. This slightly higher than expected absorption is due to the fact that the silicon that was used is actually low doped, rather than intrinsic, giving it a higher conductivity and hence more absorption.

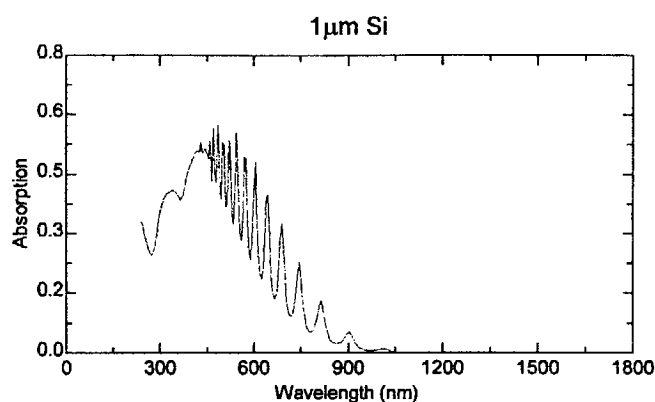


Fig. 6. Absorption of 1  $\mu\text{m}$  silicon as a function of wavelength assuming a normal angle of incidence.

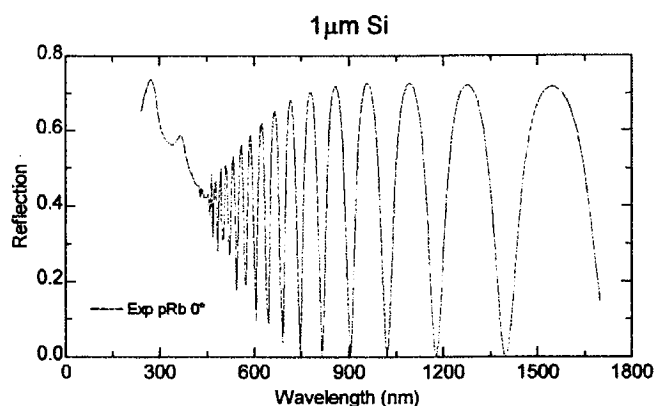


Fig. 7. Reflection of 1  $\mu\text{m}$  silicon as a function of wavelength assuming a normal angle of incidence.

### B. Thermal Transport Modes in Air

We now turn to the thermal transport parameters of the device. In air, all three transport modes (conduction, convection, and radiation) are available for carrying heat away from the beam, and hence each of these modes needs to be considered.

1) *Conduction*: Conduction is probably the simplest mechanism to consider. From Newton's law of cooling we know that conductive heat flux is given by  $\dot{q}'' = -k_{si} dT/dx$ , where  $k_{si}$  is the thermal conductivity. For silicon,  $k_{si} = k_{si}(T)$  as shown in Fig. 8 [23].

2) *Radiation*: For the special case of a grey body that is completely surrounded by a body of uniform temperature,  $T_\infty$ , the radiative heat flux is given by  $\dot{q}'' = \epsilon \sigma (T^4 - T_\infty^4)$  where  $\epsilon = \epsilon(T)$  is the total emissivity [35]. This temperature dependence is shown in Fig. 9.

3) *Convection*: The convective heat flux law is given by  $\dot{q}'' = h(T - T_\infty)$  where  $h$  is the heat transfer coefficient. In order to estimate  $h$  we assume that all of the convection takes place from the sides of the beam, and not from the top and bottom, since the aspect ratio of the beam to be used in the experiment is greater than 10 to 1.

The first step is to determine whether the air flow generated by the heated beam will be laminar or turbulent. For free convection this requires us to determine the Rayleigh number,  $Ra = Gr Pr$ . Here,  $Pr = \nu \rho c_p / k_{air}$  is the Prandtl number, which is the ratio of momentum diffusivity to thermal diffu-

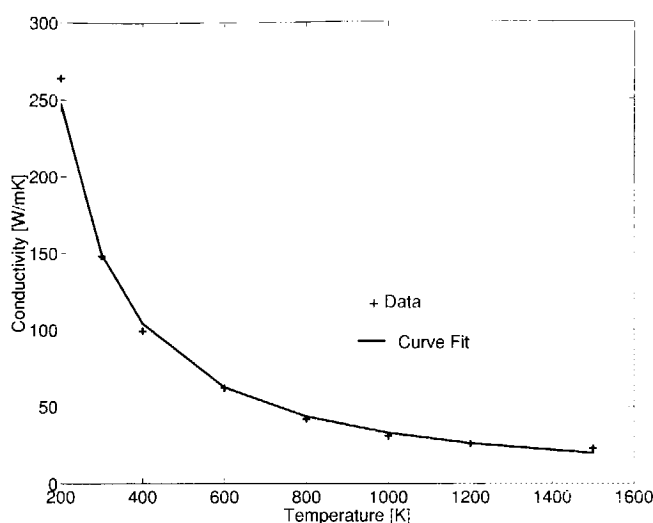


Fig. 8. Thermal conductivity of silicon as a function of temperature.

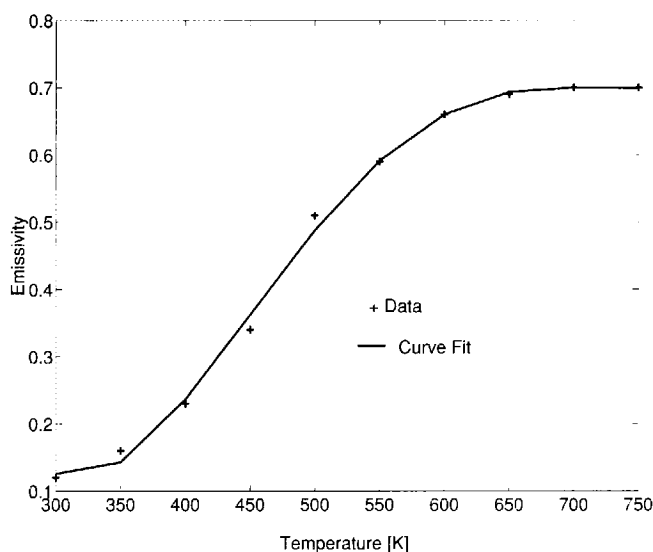


Fig. 9. Total emissivity of low-doped silicon as a function of temperature.

sivity. It turns out to be about 0.7 for air over a wide range of temperature.  $Gr = g\beta\Delta TL_c^3/\nu^2$ , is the Grashoff number. In this equation,  $g$  is the acceleration of gravity,  $\beta$  is the buoyancy coefficient ( $\beta = 1/T$  for ideal gases),  $L_c$  is the characteristic length of the surface ( $H$  for the beam), and  $\nu$  is the kinematic viscosity of air. Even in the most extreme case in which the temperature of the beam reaches the melting point of silicon we find that  $Ra \ll 1$ , and since a free convective flow does not become turbulent until  $Ra$  exceeds  $10^9$ , we see that the flow is totally laminar [23].

Given that the flow is laminar, the next step is to find the Nusselt number

$$Nu = hL_c/k_{air}. \quad (6)$$

Here,  $k_{air}$  is the thermal conductivity of the air, not the silicon. For laminar free convective flow over a vertical plate, the Nusselt number is given by

$$Nu = 0.68 + \frac{0.67Ra^{1/4}}{[1 + (0.492/Pr)^{9/16}]^{4/9}}. \quad (7)$$

TABLE I  
HEAT TRANSFER IN MILLIWATTS FOR ALL THREE MECHANISMS UNDER  
VARIOUS CONDITIONS

$t$ [ $\mu$ s]	conduction [mW]			convection [mW]			radiation [mW]		
	10	100	st. st.	10	100	st. st.	10	100	st. st.
$q_l$ [mW]									
25	0.34	0.36	0.37	$4.2 \times 10^{-3}$	0.038	0.14	$3.6 \times 10^{-6}$	$3.3 \times 10^{-6}$	$1.2 \times 10^{-4}$
200	2.7	2.9	3.0	0.033	0.303	1.2	$3.0 \times 10^{-5}$	$3.7 \times 10^{-4}$	$4.5 \times 10^{-3}$
750	10	11	11	0.13	1.1	5.6	$1.8 \times 10^{-4}$	$9.7 \times 10^{-3}$	0.43

st. st. = steady state

(See [23].) Here,  $Ra \ll 1$ , so that  $Nu \approx 0.68$ . Thus, from (6),  $h \approx 880 \text{ W/m}^2\text{K}$  which is remarkably large for a free convection coefficient.

4) *Relative Importance:* In order to see if any of the heat transfer modes may be neglected we need to calculate some typical values of heat flux for each of the mechanisms. We will consider three different laser power inputs of 25 mW, 200 mW, and 750 mW. In addition, since the temperature profile (and hence the temperature gradient) of the beam varies with time, we will also consider the heat transfer at three different times, corresponding to 10  $\mu$ sec, 100  $\mu$ sec, and steady state. All of these results are summarized in Table I. Here, the heat transfer problem is solved from Equation (3) to obtain the temperature profile of the beam as a function of time. The heat loss by each mode is then determined for the entire length of the beam. Note that for low power input and short time, conduction is the dominant mode. As time and energy input increase, convection starts to become significant. And for very high temperatures, radiation starts to become important. Thus, all three heat transfer modes need to be taken into account.

### C. Model Results

With all of the parameters determined, and a notion of the importance of the various heat transfer modes, it is possible to run the model for our bistable MEMS device. Note that here,  $q_l$  is not prescribed (in contrast to Table I), but is based on absorption of radiation energy by silicon. Fig. 10 shows the results of the model when the beam is irradiated with a 100 mW 1064 nm laser. The temperatures are low enough in this case that only conduction and convection are important.

Fig. 11 shows that the steady-state temperature at the center of the beam increases as a function of laser power. Since the melting point of silicon is 1687 K, it is clear from the figure that the laser power must be kept below about 800 mW, or the beam will melt. In fact, when a laser power of slightly over 800 mW was used, the beam did indeed melt, as can be seen in Fig. 12. Notice how the silicon has pulled into a cylindrical shape in the melt zone due to surface tension, indicating that melting rather than ablation has taken place.

## V. EXPERIMENT

Now that the theoretical foundation for optical actuation has been laid out, and the bounds on the practical operating range of this mechanism have been established, we may proceed to test its practicality by experiment.

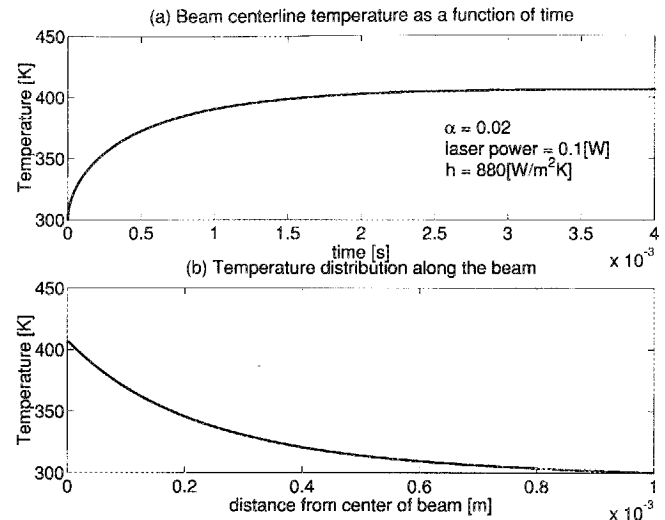


Fig. 10. (a) Temperature at the middle of the beam ( $x = 0$ ) as a function of time. (b) Temperature profile at steady state.

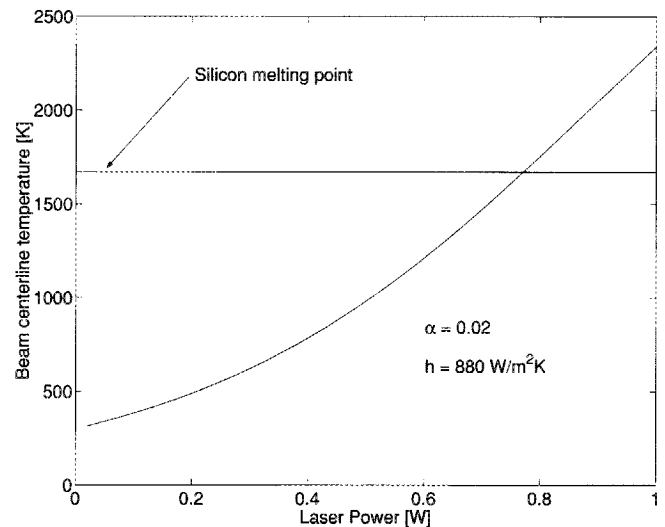


Fig. 11. Steady-state beam centerline temperature as a function of laser power.

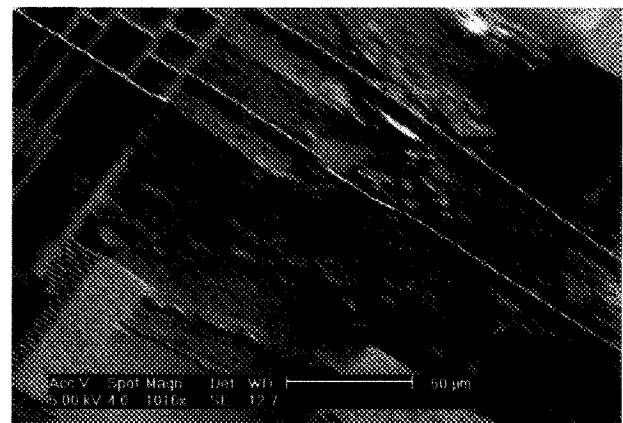


Fig. 12. Scanning electron micrograph (SEM) of a melted bistable MEMS device.

### A. Experimental Setup

The experimental setup designed to demonstrate the feasibility of toggling the silicon beam using light is illustrated in

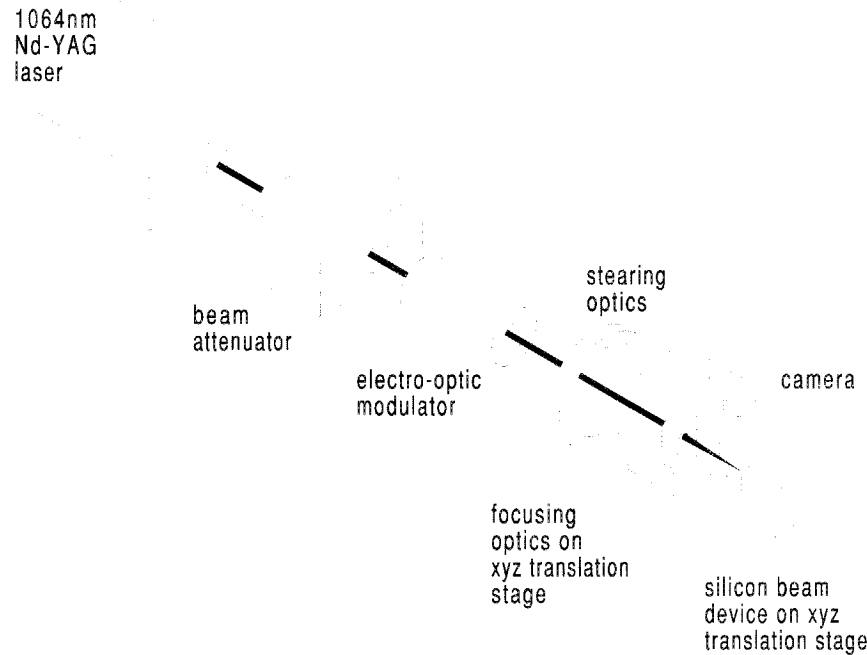


Fig. 13. Experimental setup.

Fig. 13. In this setup, a beam of 1064 nm infrared laser light generated by a Nd:YAG continuous wave laser operating at about 3 W of output power is fed into a beam attenuator and a set of filters. The output of the laser is most stable when operated at relatively high power. This laser is used because it is powerful enough to switch the state of the MEMS beam from a range of buckled states, and is reasonably reflective (72%) with very little absorption (2%) to silicon that is  $1\text{ }\mu\text{m}$  thick. The filters are used for discrete, coarse adjustment on the laser power, and the attenuator is used to fine tune the power level. The beam then enters an electrooptic modulator, which is used as a shutter for the laser beam. It is controlled digitally, blocking most of the laser power while receiving a logic low input, and passing most of the laser power while receiving a logic high input. The input signal is supplied by a square wave function generator for tuning purposes, and by a single shot bounceless switch with adjustable pulse duration during actual operation of the experiment.

From the modulator, the beam is fed into a thermal power meter on a removable quick-connect stand (this meter is not shown in the figure) in order to determine the actual laser power being sent to the MEMS beam. This power meter is removed before sending the actual toggle pulse in the experiment. From there, the laser light passes through a system of lenses used to steer the beam, and then it enters an objective lens, used to focus the light onto the side of the MEMS beam. Both the objective lens and the MEMS device are placed on micrometer controlled *xyz* translation stages for maximum flexibility in focusing the laser light on the side of the beam. A CCD camera with a microscope objective is mounted above the MEMS device in order to view the device during operation.

### B. Experimental Results

Fig. 14 shows the experimental results on the switching of the silicon beam by the laser. Here, the beam is first buckled

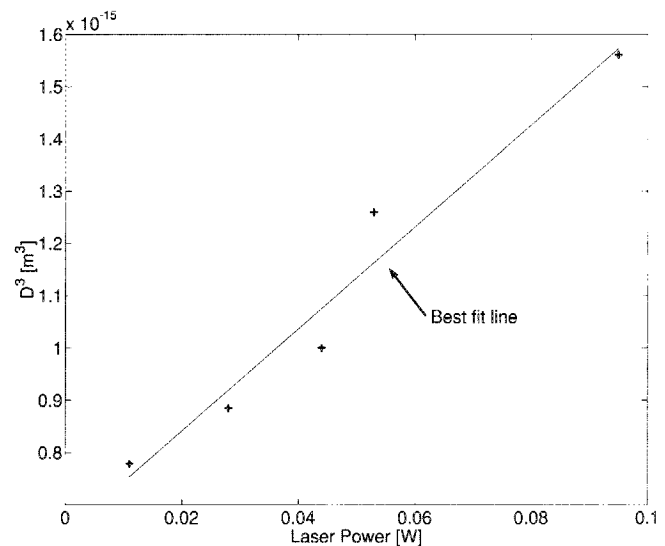


Fig. 14. Plot of beam buckle displacement cubed ( $D^3$ ) versus laser power toggle threshold.

by a displacement,  $D$ , by the compressive force actuator. The laser is then turned on for 20 msec with increasing power until switching occurs. The figure shows  $D^3$  as a function of the threshold laser power. A linear relationship is observed just as predicted in [31], since the light force is proportional to its power. Here, the offset of the straight line is attributed to an initial asymmetry of the device under test. The minimum threshold laser force applied in this experiment for  $D = 9.2\text{ }\mu\text{m}$  is around 70 pN when the laser power is 11 mW.

### C. Other Possible Mechanisms

Clearly, the experimental results presented in Fig. 14 strongly support the hypothesis that radiation pressure is the forcing mechanism responsible for the toggling of the beam. However,

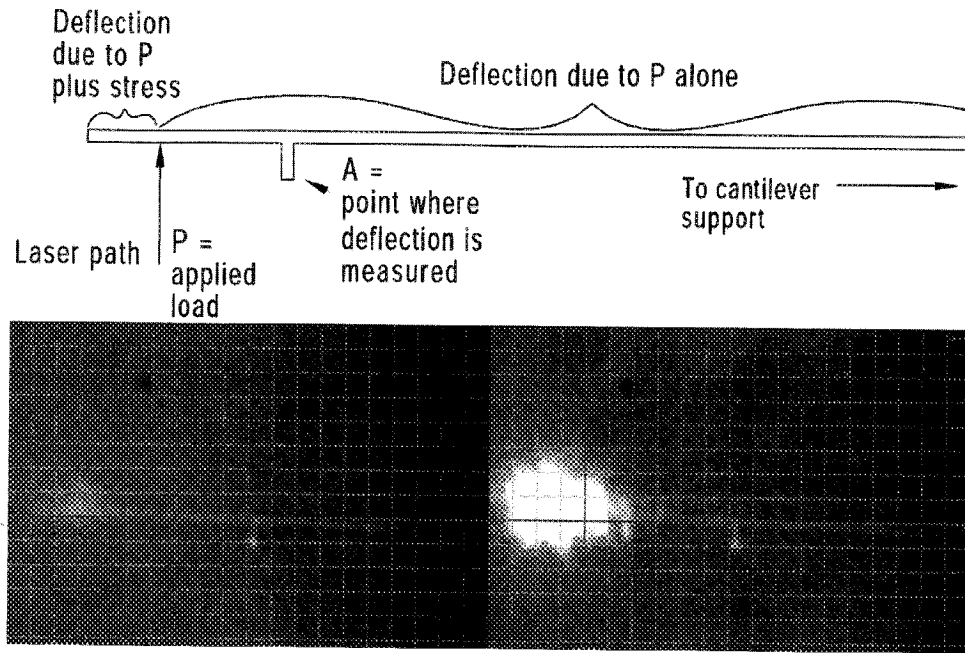


Fig. 15. The illustration at the top shows the portion of the cantilever beam pictured in the images below it. The image at left shows the cantilever tip before illumination by the laser, and the image at right shows the deflection of the cantilever while illuminated. The grid size is approximately  $5\ \mu\text{m}$ .

other mechanisms might also be responsible for toggling the beam, and need to be explored in order to determine their feasibility.

1) *Beam Heating*: A simple thought experiment shows that this mechanism could not toggle the beam with the experimental setup used in this paper. Heating the beam causes it to expand. This expansion, in turn, causes additional compressive stress in the beam, which would result in the beam buckling even more. It could not possibly cause it to toggle.

Even if differential heating from one side of the beam to the other is considered the situation remains the same. Since the beam is incident on the outside of the buckled curve, the moment imparted by the heating would reinforce, rather than counteract the buckle in the beam. Thus, heating cannot be responsible for the toggle of the beam.

2) *Photo-Induced Stress*: A far less obvious possible mechanism for toggling the beam is the photo-induced stress caused by photo-generated charge carriers in semiconductors. This mechanism has been used by [18] in a high sensitivity photon detector. As a semiconducting cantilever absorbs a photon the resulting strain causes bending which can be measured by optical, piezoresistive, or capacitive means. And it turns out that for silicon, the photo-induced stress is tensile (i.e., it contracts the lattice), and about four times as large as the thermal stress in the area of direct absorption. However, since this mechanism relies on absorption (it is the generation of electron-hole pairs due to absorption that generates the strain), and we have specifically set up our experiment to minimize absorption, this mechanism is not believed to be responsible. However, the experiment presented in this paper is insufficient to rule it out.

In order to eliminate photo-induced stress as a possibility, a second experiment was conducted using  $1.3\ \mu\text{m}$  laser light on a simple silicon cantilever beam. The higher wavelength reduces

the absorptivity of the low doped silicon by a factor of four. And for a cantilever, the deflected shape of the beam from the support to the point of applied load is independent of the local longitudinal stress state of the beam at the load point, whether that stress be thermally generated or photo-induced.

For a cantilever beam, the spring constant for a concentrated load at a point at a distance  $L$  from the support is given by

$$k = \frac{EHB^3}{4L^3} \quad (8)$$

where  $E$  is the elastic modulus, and  $H$ ,  $B$ , and  $L$  are the height, width, and length, respectively, of the beam. The experiment was conducted on a silicon beam with nominal dimensions of  $10\ \mu\text{m} \times 1\ \mu\text{m} \times 1000\ \mu\text{m}$ , and an elastic modulus of 170 GPa. The laser was focused on the lateral surface of the cantilever at a point  $990\ \mu\text{m}$  from the support, giving the cantilever a spring constant of  $440\ \mu\text{N/m}$ . The laser being used was approximately 200 mW at a wavelength of 1316 nm, giving it a reflectivity of 0.65. In addition, it intersected the silicon beam at an angle of incidence of about  $10^\circ$ , and the focused spot size was such that only about 70% of the light actually intercepted the beam, which generates a total load,  $P$ , of 0.6 nN on the beam.

A point,  $A$ , on the cantilever at a distance,  $x$ , from the support should be deflected by

$$y = \frac{12P}{EHB^3} \left( L \frac{x^2}{2} - \frac{x^3}{6} \right). \quad (9)$$

We observed the deflection of the cantilever at a distance of  $x = 960\ \mu\text{m}$  from the support to be about  $0.9\ \mu\text{m}$ . The experiment is shown in Fig. 15 (while the deflection is very small, it can be seen with the aid of the  $5\ \mu\text{m}$  grid). From Equation (9), the expected deflection due to radiation pressure is  $1.3\ \mu\text{m}$ , which is in reasonable agreement with the experimental results. Here, the deflection of point  $A$  is not influenced by photo-induced or non-uniform thermal stress since  $A$  is between the support and the

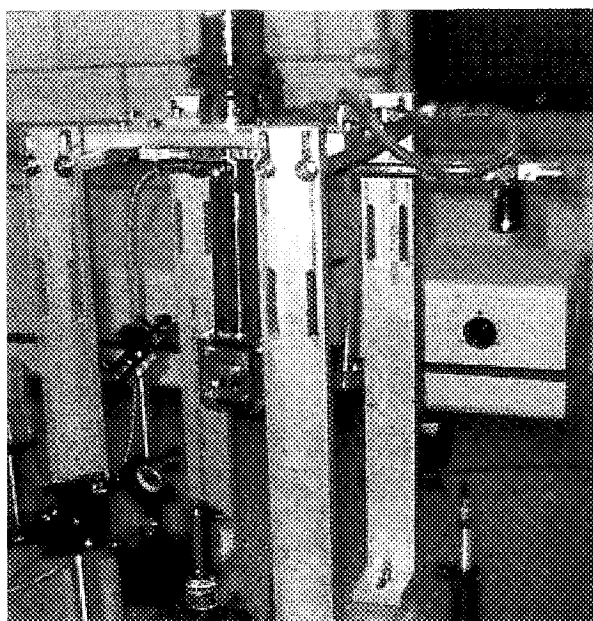


Fig. 16. Image of the vacuum chamber used to test optical actuation in vacuum.

region of incident illumination. These stress induced effects can only influence the deflection of the beam beyond the illuminated region. The agreement between theory and experiment for the cantilever reinforces the argument that radiation pressure was the dominant forcing mechanism in the bistable experiment.

3) *Ablation*: Ablation works by heating the silicon at the surface of the beam past its boiling point (3538 K) so that the material flashes to vapor and is ejected from the surface. The use of ablation as a propulsion mechanism is well established [29]. This mechanism is by far the least desirable of all those identified in this paper, since it results in damaging the beam. While the wavelength used in this experiment was chosen because it coincided with a reflection maximum for the beam and it appeared to have very low absorption, it is still close enough to the bandgap of silicon to cause some concern. Future experiments will be conducted using 1.3 micron laser light, in order to be comfortably below this bandgap. For the experiments already conducted, the best that can be said is that the MEMS device was subjected to a large number of laser pulses in the same spot without any visual indication of surface damage. Furthermore, no damage was apparent and no failures occurred up to the point at which the thermal model predicted that the beam should melt. Thus, it is doubtful that ablation is responsible for toggling the beam.

4) *The Radiometer Effect*: In this mechanism, the silicon absorbs energy from the light, causing it to heat. The heating of the silicon, in turn, heats the air around it, causing the air to expand. The expansion of the air around the beam exerts a pressure on it, causing it to move. The radiometer effect was the dominant source of error in early experiments which attempted to demonstrate the momentum of light [4], and hence it cannot be ignored. However, we note that pressure (and hence force) is a linear function of temperature for an ideal gas such as air, and the functional relationship between laser power and temperature is decidedly nonlinear (see Fig. 11). Hence we should

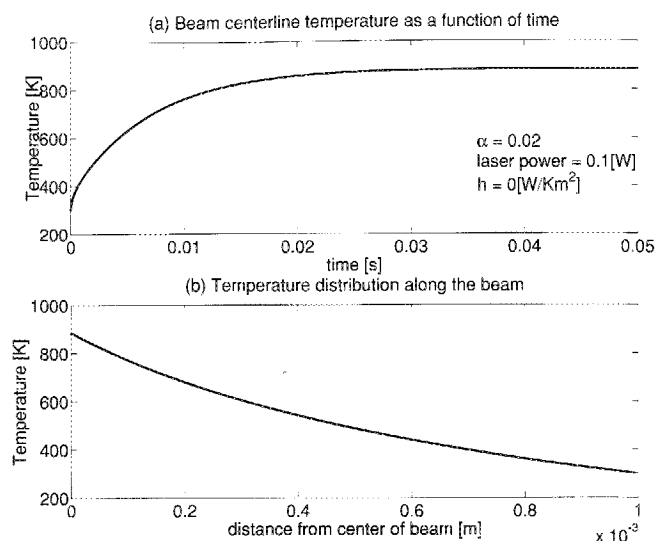


Fig. 17. (a) Temperature in vacuum at the middle of the beam ( $x = 0$ ) as a function of time. (b) Temperature profile at steady state in vacuum.

expect the force (which we know to be proportional to  $D^3$ ) to be a nonlinear function of laser power for the radiometer effect. But our experiment showed that the actual force provided by the laser was indeed linear with laser power, which is what we would expect for radiation pressure. Nevertheless, the possibility of this forcing mechanism is strong, and so the toggling experiment was carried out in vacuum where the radiometer effect would be absent. (Fig. 16 shows the vacuum chamber.)

We find that again, the beam toggles in vacuum at the power levels predicted using radiation pressure, implying that radiation pressure is the dominant mechanism. However in vacuum, heating of the beam is of prime importance due to the lack of convection. Fig. 17 shows the thermal model prediction of temperature rise in the beam due to 100 mW incident laser power in vacuum. Note that the steady state temperature rise at the center of the beam is nearly six times larger in vacuum than it was in air. In fact, the thermal model, with the convective term removed, predicted that melting would occur at a power level of 175 mW if the beam temperature were initially elevated to 1100 K by the incandescent illumination used to image the beam. This can occur in vacuum. There is no convection. The temperature is not high enough for appreciable radiation, and the MEMS device used in these experiments cannot conduct much heat away since it is mounted on a polymer substrate. After functioning for a time in vacuum, the beam did indeed melt upon being hit with a 175 mW laser pulse.

## VI. CONCLUSION

This paper has presented an actuation mechanism for MEMS devices based on the pressure exerted by incident radiation. Several possible attractive features of this actuation scheme have been identified, including scaling, interconnectivity, and the ability to operate in harsh environments. The practical limitations of the optical actuation have been explored, including collimation issues and potential thermal problems. Finally, the mechanism has been experimentally demonstrated by toggling the state of a bistable MEMS device, both in air and in vacuum

by using radiation pressure. It is shown that there are several forcing mechanisms that may be activated due to radiation, but the radiation force is by far the most dominant one. A thermal model to estimate the temperature rise in a MEMS silicon beam due to radiation is carried out. It is shown that the magnitude of optical force is limited primarily by the temperature rise of the MEMS device due to absorption of radiation energy.

#### ACKNOWLEDGMENT

The laser experiments were performed in the FSMRL laser facility. The authors would also like to thank Dr. T. H. Wood and Lucent Technologies for the donation of the Nd : YAG laser used for this experiment.

#### REFERENCES

- [1] M. Born and E. Wolf, *Principles of Optics*. London: Pergamon Press, Ltd., 1959.
- [2] M. Q. Brewster, *Thermal Radiative Transfer and Properties*. New York: Wiley, 1992.
- [3] B. Culshaw, "Optically excited resonant sensors," *Fiber Optic Sensors*, pp. 33–44, 1987.
- [4] R. W. Ditchburn, *Light*. New York: Interscience, 1953.
- [5] D. Dragoman and M. Dragoman, "Optical actuation of micromechanical tunneling structures with applications in spectrum analysis and optical computing," *Appl. Optics*, vol. 38, no. 32, pp. 6773–6778, 1999.
- [6] E. Palik, Ed., *Handbook of Optical Constants in Solids, III*. San Diego, CA: Acad. Press, 1998.
- [7] A. L. Smirl *et al.*, "Pulsewidth dependence of nonlinear energy deposition and redistribution in Si, gas, and Ge, during 1-micrometer picosecond irradiation," *J. Lumin.*, vol. 30, p. 272, 1985.
- [8] D. Dieulesaint *et al.*, "Mechanical excitation of a membrane by an optical beam," in *1981 Ultrasonics Symp.*, 1981, pp. 802–805.
- [9] D. Uttamchandani *et al.*, "Optically excited resonant beam pressure sensor," *Electron. Lett.*, vol. 23, pp. 1333–1334, 1987.
- [10] E. Roan *et al.*, "Optically actuated all optical mechanical switch," in *LEOS 2000 IEEE Annual Meeting Conf. Proc. 13th Annual Meeting*, vol. 2, 2000, pp. 641–642.
- [11] J. Yang *et al.*, "Surface effects and high quality factors in ultrathin single-crystal silicon cantilevers," *Appl. Phys. Lett.*, vol. 77, no. 23, pp. 3860–3862, 2000.
- [12] J. D. Zook *et al.*, "Optically excited self-resonant microbeams," *Sens. Actuators, A*, vol. 52, no. 1–3, pp. 92–98, 1996.
- [13] K. E. B. Thornton *et al.*, "Temperature dependence of resonant frequency in optically excited diaphragms," *Electron. Lett.*, vol. 22, pp. 1232–1234, 1986.
- [14] M. V. Andres *et al.*, "Analysis of an interferometric optical fiber detection technique applied to silicon vibrating sensors," *Electron. Lett.*, vol. 22, pp. 1097–1099, 1986.
- [15] M. V. Andres *et al.*, "Analysis of an interferometric optical fiber detection technique applied to silicon vibrating sensors," *Electron. Lett.*, vol. 23, pp. 774–775, 1987.
- [16] M. Zalalutdinov *et al.*, "Autoparametric optical drive for micromechanical oscillators," *Appl. Phys. Lett.*, vol. 79, no. 5, pp. 695–697, 2001.
- [17] M. Zalalutdinov *et al.*, "Optically pumped parametric amplification for micromechanical oscillators," *Appl. Phys. Lett.*, vol. 78, no. 20, pp. 3142–3144, 2001.
- [18] P. G. Datskos *et al.*, "Detection of photons using the electronic stress in metal semiconductor interfaces in mems devices," *Appl. Phys. Lett.*, vol. 73, pp. 2319–2321, 1999.
- [19] R. E. Jones *et al.*, "Optical fiber sensors using micromachined silicon resonant elements," *IEEE Proc. Part D*, vol. 135, no. 5, pp. 353–358, 1988.
- [20] S. Thakoor *et al.*, "Optical microactuation in piezoceramics," *Proc. of SPIE—Int. Soc. Opt. Eng.*, vol. 3328, pp. 376–391, 1998.
- [21] W. Benecke *et al.*, "Optically excited mechanical vibrations in micro-machined silicon cantilever structures," in *Proc. 3rd Int. Conf. Solid-State Sensors and Actuators (Transducers '87)*, 1987, pp. 838–848.
- [22] R. P. Feynman, *The Feynman Lectures on Physics*. Palo Alto, CA: Addison-Wesley, 1963.
- [23] F. P. Incropera and D. P. Dewitt, *Introduction to Heat Transfer*. New York: Wiley, 1996.
- [24] ———, *Fundamentals of Microfabrication*. New York: CRC, 1997.
- [25] D. R. Koehler, "Optical actuation of micromechanical components," *J. Opt. Soc. Amer. B: Opt. Phys.*, vol. 14, no. 9, pp. 2197–2203, 1997.
- [26] J. C. Maxwell, *A Treatise on Electricity and Magnetism*. Oxford, U.K.: Clarendon, 1873.
- [27] J. R. Meyer, F. J. Bartoli, and M. R. Kruer, "Optical heating in semiconductors: Laser damage in Ge, Si, InSb, and GaAs," *J. Appl. Phys.*, vol. 51, no. 10, pp. 5513–5522, 1980.
- [28] E. F. Nichols and G. F. Hull, "A preliminary communication on the pressure of heat and light radiation," *Phys. Rev.*, vol. 13, pp. 307–320, 1901.
- [29] A. V. Pakhomov and D. A. Gregory, "Ablative laser propulsion: An old concept revisited," *AIAA Journal*, vol. 38, no. 4, pp. 725–727, 2000.
- [30] S. A. Parvez, "Solar pressure disturbance on GPS and spacenet satellites," *J. Spacecraft Rockets*, vol. 19, no. 3, pp. 482–488, 1994.
- [31] M. T. A. Saif and N. R. Miller, "Modeling and analysis of a tunable bistable mems for opto-mechanical computational logic elements," in *Proc. ASME IMECE'99-MEMS*, vol. 1, 1999, pp. 31–36.
- [32] M. Schwarzschild, *Structure and Evolution of the Stars*. Princeton, NJ: Princeton University Press, 1958.
- [33] A. E. Siegman, *Lasers*. Mill Valley, CA: University Science Books, 1986.
- [34] B. G. Streetman, *Solid State Electronic Devices*. Englewood Cliffs, NJ: Prentice Hall, 1995.
- [35] P. J. Timans, "Emissivity of silicon at elevated temperature," *J. Appl. Physics*, vol. 74, no. 10, pp. 6353–6364, 1993.
- [36] W. Trimmer, "Microbots and micromechanical systems," *Sens. Actuators, Phys. A*, vol. 19, pp. 267–287, 1989.
- [37] S. Venkatesh and B. Culshaw, "Optically activated vibrations in a micro-machined silica structure," *Electron. Lett.*, vol. 21, pp. 315–317, 1985.

**Marc Sulfridge** received the B.S. degree in engineering and applied science from the California Institute of Technology (Caltech), Pasadena, in June of 1996. He received the M.S. degree in mechanical and industrial engineering from the University of Illinois, Urbana-Champaign (UIUC), in October of 1998. He is currently a graduate student at the University of Illinois and plans to defend his doctoral dissertation in December of 2002.

He has worked on a number of research projects while attending UIUC, including control oriented modeling of vapor compression cycles, MEMS scale cooling systems, and the optical actuation of MEMS devices.

**Taher Saif** received the B.S. and M.S. degrees in civil engineering from Bangladesh University of Engineering and Technology and Washington State University in 1984 and 1986, respectively. He received the Ph.D. degree in theoretical and applied mechanics from Cornell University, Ithaca, NY, in 1993.

He worked as a Postdoctoral Associate in electrical engineering and the National Nanofabrication Facility at Cornell University from 1993 to 1997. He joined the Department of Mechanical and Industrial Engineering at the University of Illinois, Urbana-Champaign (UIUC), during 1997 as an Assistant Professor. His current research projects include actuation of MEMS by light beams, mechanical behavior of nanoscale materials, interaction between small thin plates forming menisci with a fluid, and mechanical response of single living cells due to local deformations.

**Norman Miller** received the B.S. degree in mechanical engineering from the University of Missouri, Rolla, in 1968. He received the Ph.D. degree in mechanical engineering from the University of Wisconsin, Madison, in 1976.

In 1976, he joined the Department of Mechanical and Industrial Engineering at the University of Illinois at Urbana-Champaign. In the early 1980s, he was a Founder of SoMat Corporation, an instrumentation company in Urbana, IL, that was recently acquired by AEA Technologies. He continues to serve as a member of the board of directors of SoMat. His current research projects include actuation of MEMS devices by light beams and acoustic phenomena in refrigeration systems.

**Keith O'Hara** received the B.S. degree in engineering physics from the Ohio State University in 1989 and the Ph.D. degree in physics from the University of Illinois, Urbana-Champaign (UIUC), in 1998.

He then served on Scientific Staff of the Materials Research Laboratory at the University of Illinois. His current work at Integrated Micromachines, Monrovia, CA, is focused on bringing MEMS to the telecommunications industry.